(Received 5 July 2024, Accepted 12 August 2024, Scheduled 23 August 2024)

Wideband Unequal Four-Way Filtering Power Divider with Absorptive Feature

Shuyi Chen, Hongmei Liu*, Teng Ma, and Zhongbao Wang

School of Information Science and Technology, Dalian Maritime University, Dalian, Liaoning 116026, China

ABSTRACT: In the paper, a wideband four-way filtering power divider with arbitrary power division ratio and input absorptive feature is proposed. Two sets of coupled lines (CLs) are used to achieve the wideband performance. To obtain absorptive properties, a set of T-type absorption structure consisting of two isolation resistors and a $\lambda/4$ short-circuit stub is connected between the two CLs. Meanwhile, high frequency selectivity and good out-of-band rejection are realized by introducing two stepped-impedance resonators. Besides, output impedance matching, isolation, and unequal power distribution are achieved by the power division section in the second stage. In the analysis, the equations are derived by using the method of even-odd mode decomposition and voltage-current method. For demonstration, a prototype is designed, fabricated, and measured with the power distribution ratio of $2:1:1:2$. Measurements show that an all-frequency band absorption of 200% is obtained with the 3-dB passband bandwidth of 78.1% and out-of-band rejection of 14 dB. Besides, it also shows 15-dB isolations within more than 60% FBW and has the feature of small size.

1. INTRODUCTION

Wideband power dividers [1, 2] have become a research hotspot in recent years. The wideband filtering power dividers (FPDs) with integrated multi-way output [3–7], unequal power distribution [8–11], and all-frequency band absorptive feature [12–17] have become the top priority of research.

Reports have been exhibited to design wideband FPDs with different structures. For example, in [3], a class of $2n$-way wideband FPDs with a fractional bandwidth (FBW) of 106% is proposed. In order to availably enlarge the isolation bandwidth, an isolation network is first implied to replace the isolation resistor of the traditional Wilkinson power divider. In [4], an asymmetric three-way equal wideband FPD with apparent selectivity is proposed. The proposed three-way PD has a compact size, low insertion loss (IL), good return loss (RL), sharp selectivity, wide FBW, and filtering functions. In [8], a wideband unequal FPD with arbitrary constant power ratio and phase difference is designed. The results show that the structure has a PDR of $4:1$ with a 90° phase difference, and it can reach a relative bandwidth of 53%. However, this work has a defect of poor frequency selectivity. In [10], the paper introduces the design and practical implementation of a non-reciprocal FPD with an arbitrary PDR and tunable central frequency. The results show that the structure has a relative bandwidth of 17.6%, a maximum forward insertion loss of 4.95 dB, and more than 20 dB isolation.

However, the unemitted RF-input signals in the stopband will be reflected back to the source and affect the performance of the circuit. Thus, the FPDs with absorptive feature can be a good solution to deal with this problem. So far, a few researches have been reported on absorptive FPDs. In [13], by using a composite T-type network consisting of a set of resistors and a $\lambda/4$ shorted stub, good isolation and input absorptive feature are realized. To enhance the absorptive effect, an additional absorptive stub is added to the input port. The proposed absorptive FPD has all-band input-reflectionless property, showing a wide 1-dB FBW of 52.8%, the minimum in-band IL of 0.32 dB, and more than 16 dB isolation. In [17], three simple absorptive stubs composed of $\lambda/4$ shorted stubs series with resistors are applied to realize all-frequency absorption of the RF-input-power. Although these FPDs achieve good absorption and filtering features, they have only two-way output ports. Therefore, it is still difficult to design absorptive FPDs with multi-way output and unequal power distribution.

In this paper, a wideband four-way FPD with arbitrary power division ratio (PDR) and input absorptive feature is proposed. It has the merits of (1) unequal power division, (2) wide FBW for all-ports return losses and isolations, (3) input absorptive feature, (4) good out-of-band suppression. This paper is organized in 4 sections. Section 1 describes the current research status and advantages of wideband filtering power divider. In Section 2, the analytical process and design formula are given for the proposed FPD. For demonstration, a prototype is provided in Section 3, followed by the conclusion in Section 4.

2. THEORETICAL ANALYSIS

Figure 1 shows the structure of the proposed wideband unequal four-way FPD. It consists of two sets of coupled lines (CLs), a T-shape absorptive stub, two stepped-impedance resonators (SIRs), and two sets of power division section. The CLs have the even- and odd-mode characteristic impedances of Z_e and Z_o, respectively, with an electrical length of θ. The T-shape absorptive stub consists of two resistors named R_1 and a short-

* Corresponding author: Hongmei Liu (lhm323@dlmu.edu.cn).

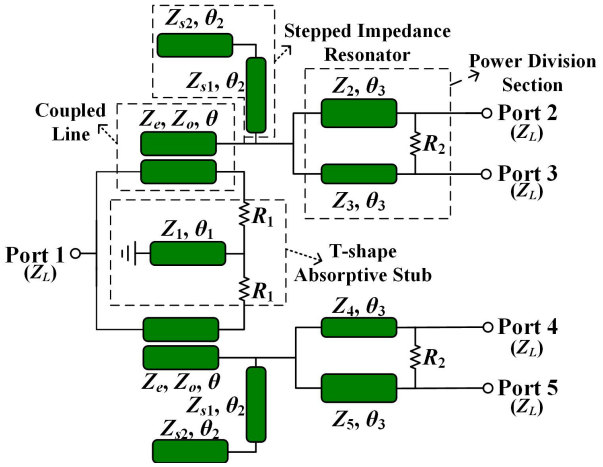

FIGURE 1. Schematic of the proposed wideband unequal four-way FPD.

circuit transmission line (TL) with the impedances of Z_1. The SIR is constructed by two TLs with the impedances of Z_{s1} and Z_{s2}. The power division section consists of two TLs with the impedances of Z_2 and Z_3. Besides, one resistor R_2 is linked between two TLs to achieve good isolation between adjacent output ports. It is noted that the electric length of each section is assigned as 90° at the center frequency ($\theta_1 = \theta_2 = \theta_3 = \theta = 90°$).

For simplified analysis, the relations of $Z_3 = Z_4$ and $Z_2 = Z_5$ are assigned. Thus, the even-odd mode decomposition method can be applied. Fig. 2 exhibits the even- and odd-mode sub-circuits. When assuming the PDR of the FPD as k^2, the output ports power ratio is $k^2 : 1 : 1 : k^2$ corresponding to ports 2, 3, 4, and 5.

Firstly, the reflection coefficient S_{11} is derived. Since the proposed structure is symmetric, and the power division ratio for port 2 and 3 is $k^2 : 1$, the impedances of the TLs in the power division section should satisfy the following relations [11].

$$Z_3 = k^2 Z_2 \quad Z_4 = k^2 Z_5 \tag{1}$$

According to the even-mode shown in Fig. 2(a), the impedance seen from port 1 (Z_{ine1}) can be derived as (2).

$$Z_{ine1} = Z_{11} + \frac{Z_{44}^2 (Z_{11} + Z_a) + Z_{33}^2 (Z_{11} + Z_{in2}) - 2Z_{22}Z_{33}Z_{44}}{Z_{22}^2 - (Z_{11} + Z_a)(Z_{11} + Z_{in2})} \tag{2}$$

where

$$Z_{11} = -\mathrm{j}\frac{Z_e + Z_o}{2}\cot\theta \quad Z_{22} = -\mathrm{j}\frac{Z_e - Z_o}{2}\cot\theta$$
$$Z_{33} = -\mathrm{j}\frac{Z_e - Z_o}{2}\csc\theta \quad Z_{44} = -\mathrm{j}\frac{Z_e + Z_o}{2}\csc\theta \tag{3a}$$

$$Z_a = R_1 + \mathrm{j}2Z_1\tan\theta_1 \tag{3b}$$

$$Z_{in2} = \frac{Z_k Z_{in4}}{Z_k + Z_{in4}} \tag{3c}$$

and

$$Z_k = \frac{\mathrm{j}Z_{s1}(Z_{s1}\tan\theta_2 - Z_{s2}\cot\theta_2)}{Z_{s1} + Z_{s2}} \tag{4a}$$

$$Z_{in4} = \frac{1}{\frac{Z_3 + \mathrm{j}Z_L\tan\theta_3}{Z_3(Z_L + \mathrm{j}Z_3\tan\theta_3)} + \frac{Z_2 + \mathrm{j}Z_L\tan\theta_3}{Z_2(Z_L + \mathrm{j}Z_2\tan\theta_3)}} \tag{4b}$$

Thus, when ignoring the influence of the resistor R_2, S_{11} can be expressed as (5). Here, Z_L represents the impedance of each port.

$$S_{11} = \Gamma_e = \frac{Z_{ine1} - Z_L}{Z_{ine1} + Z_L} \tag{5}$$

Secondly, the S-parameters between ports 2 and 3 under even- and odd-mode excitation are derived. Fig. 3 gives the simplified equivalent circuit, where Z_{in3} and Z_{in6} are the port impedances for even- and odd-mode circuits seen from the power division section, respectively. By using the voltage-current analysis, the S-parameters [11] of the two excitation conditions can be obtained as (6).

$$S_{22e(o)} = \frac{Y_{22e(o)}Z_L + 1 - |Y_{e(o)}|Z_L^2 - Y_{11e(o)}Z_L}{Y_{22e(o)}Z_L + 1 + |Y_{e(o)}|Z_L^2 + Y_{11e(o)}Z_L} \tag{6a}$$

$$S_{32e(o)} = \frac{-2Y_{21e(o)}Z_L}{Y_{22e(o)}Z_L + 1 + |Y_{e(o)}|Z_L^2 + Y_{11e(o)}Z_L} \tag{6b}$$

$$S_{33e(o)} = \frac{-Y_{22e(o)}Z_L + 1 - |Y_{e(o)}|Z_L^2 + Y_{11e(o)}Z_L}{Y_{22e(o)}Z_L + 1 + |Y_{e(o)}|Z_L^2 + Y_{11e(o)}Z_L} \tag{6c}$$

where

$$\begin{cases} Y_{11e(o)} = \frac{\mathrm{j}Z_3 Y_{in3(6)}\sin\theta_3\cos\theta_3 - Y_2 Z_3\sin^2\theta_3 + \cos^2\theta_3}{\mathrm{j}(Z_2+Z_3)\sin\theta_3\cos\theta_3 - Z_2 Z_3 Y_{in3(6)}\sin^2\theta_3} + \frac{1}{R_2} \\ Y_{12e(o)} = -\frac{1}{\mathrm{j}(Z_2+Z_3)\sin\theta_3\cos\theta_3 - Z_2 Z_3 Y_{in3(6)}\sin^2\theta_3} - \frac{1}{R_2} \\ Y_{21e(o)} = -\frac{1}{\mathrm{j}(Z_2+Z_3)\sin\theta_3\cos\theta_3 - Z_2 Z_3 Y_{in3(6)}\sin^2\theta_3} - \frac{1}{R_2} \\ Y_{22e(o)} = \frac{\mathrm{j}Z_2 Y_{in3(6)}\sin\theta_3\cos\theta_3 - Y_3 Z_2\sin^2\theta_3 + \cos^2\theta_3}{\mathrm{j}(Z_2+Z_3)\sin\theta_3\cos\theta_3 - Z_2 Z_3 Y_{in3(6)}\sin^2\theta_3} + \frac{1}{R_2} \end{cases} \tag{7}$$

and

$$\begin{cases} Z_{in3(6)} = \frac{Z_k Z_{in1(5)}}{Z_k + Z_{in1(5)}} \\ Z_{in1(5)} = Z_{11} + \frac{Z_{44}^2(Z_{11}+Z_a(R_1)) + Z_{22}^2(Z_{11}+2Z_L(0)) - 2Z_{22}Z_{33}Z_{44}}{Z_{33}^2 - (Z_{11}+Z_a(R_1))(Z_{11}+2Z_L(0))} \end{cases} \tag{8}$$

According to (6), the S-parameters of the whole circuit can be expressed as (9)

$$S_{22} = S_{55} = \frac{S_{22e} + S_{22o}}{2} \tag{9a}$$

$$S_{33} = S_{44} = \frac{S_{33e} + S_{33o}}{2} \tag{9b}$$

$$S_{32} = S_{45} = \frac{S_{32e} + S_{32o}}{2} \tag{9c}$$

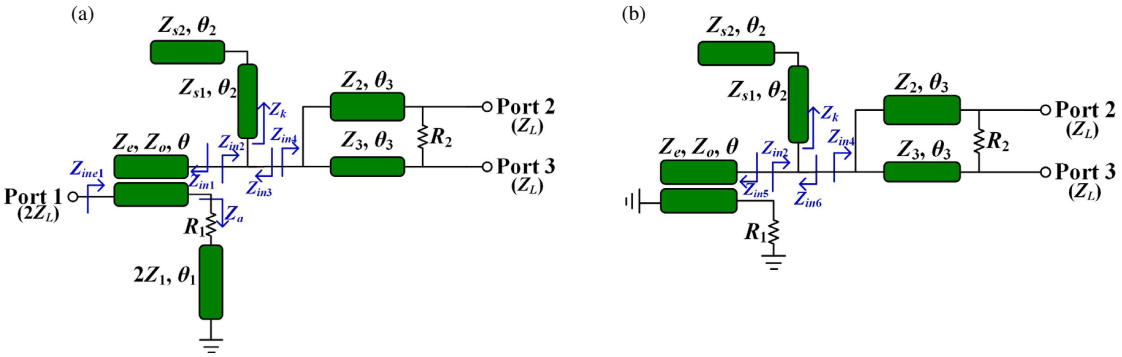

FIGURE 2. Sub-circuits of the proposed FPD. (a) Even-mode, (b) odd-mode.

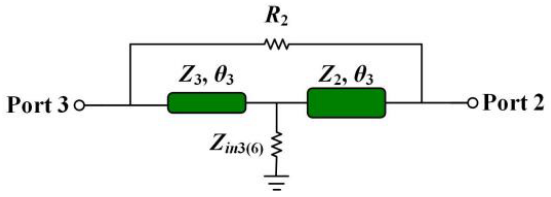

FIGURE 3. Equivalent circuit of the power division section.

$$S_{24}=S_{34}=S_{25}=S_{35}=\frac{S_{22e}-S_{22o}+S_{33e}-S_{33o}}{2} \quad (9d)$$

To obtain the circuit parameters, particle swarm optimization algorithm [18] is applied according to the S-parameter expressions. The defined objective function F is given in Equation (10)

$$\begin{aligned} &F\left(Z_e, Z_o, Z_1, Z_2, Z_3, Z_{s1}, Z_{s2}, R_1, R_2\right) \\ &= \frac{1}{N}\sum_{i=1}^{N}\left(\left|S_{11}\left(f_i\right)\right|^2+\left|S_{22}\left(f_i\right)\right|^2+\left|S_{33}\left(f_i\right)\right|^2\right. \\ &\quad \left.+\left|S_{32}\left(f_i\right)\right|^2+\left|S_{24}\left(f_i\right)\right|^2\right) \quad (10a) \end{aligned}$$

$$f_i = f_0\left(1+\frac{i-1}{D}\right) \quad (i=1,...,N) \quad (10b)$$

where f_i represents the sampling frequency; f_0/D is the sample interval; and N is the number of sampling points.

Figure 4 gives an optimization flowchart. The optimization goals are as follows: (1) the FBW of $|S_{11}| < -10$ dB is larger than 200%. (2) the overlapped FBW for 10-dB return loss (RL), 10-dB isolation, and 3-dB passband is larger than 60%. (3) Out-of-band rejection is greater than 17 dB. For illustration, an example with PDR of $2:1:1:2$ is provided. A group of optimized calculated parameters are as follows: $Z_e = 168\,\Omega$, $Z_o = 52\,\Omega$, $Z_1 = 50\,\Omega$, $Z_2 = Z_5 = 60\,\Omega$, $Z_3 = Z_4 = 120\,\Omega$, $Z_{S1} = 100\,\Omega$, $Z_{S2} = 75\,\Omega$, $R_1 = 130\,\Omega$ and $R_2 = 90\,\Omega$.

Based on the above analysis, the proposed design process of the wideband four-way FPD can be summarized as follows:

1. Determine the center frequency f_0, fractional bandwidth FBW, and dielectric constant ε_r.

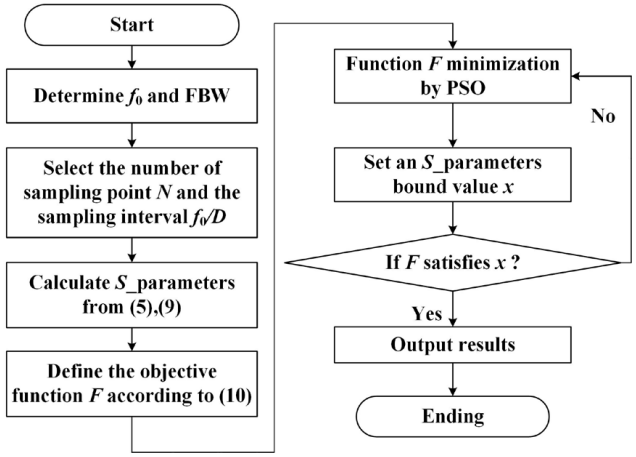

FIGURE 4. The optimization flowchart.

2. According to the optimization flowchart in Fig. 4, the impedance parameters Z_e, Z_o, Z_1, Z_2, Z_3, Z_{s1}, Z_{s2}, R_1, and R_2 can be obtained.

3. Convert the parameters into physical structure and adjust the layout of the whole circuit by electromagnetic simulation for better results.

Figure 5 shows the theory calculated results. It is observed that under the criterion of $|S_{11}| < -10$ dB, the frequency range is from 0 to $2f_0$ with the FBW of 200%. Besides, the RLs for the output ports are larger than 10 dB in the FBW of 87%. From $0.65f_0$ to $1.35f_0$ (70%), the adjacent ports isolations are greater than 14 dB. In addition, the non-adjacent ports isolations are greater than 20 dB within the whole band. Meanwhile, the 3-dB FBWs are 79%, 81%, 81%, and 79% for output ports 2, 3, 4, and 5, respectively. In addition, the out-of-band rejections are more than 18 dB.

3. IMPLEMENTATION AND RESULTS

In this section, a prototype is designed at the center frequency of 2 GHz for validation. Based on the calculated parameters, the prototype is modeled on an F4B substrate ($\varepsilon_r = 3.5$, $\tan\delta = 0.003$, $h = 1$ mm) and optimized using the Ansoft HFSS. Fig. 6 shows the layout and photograph of the fabricated prototype,

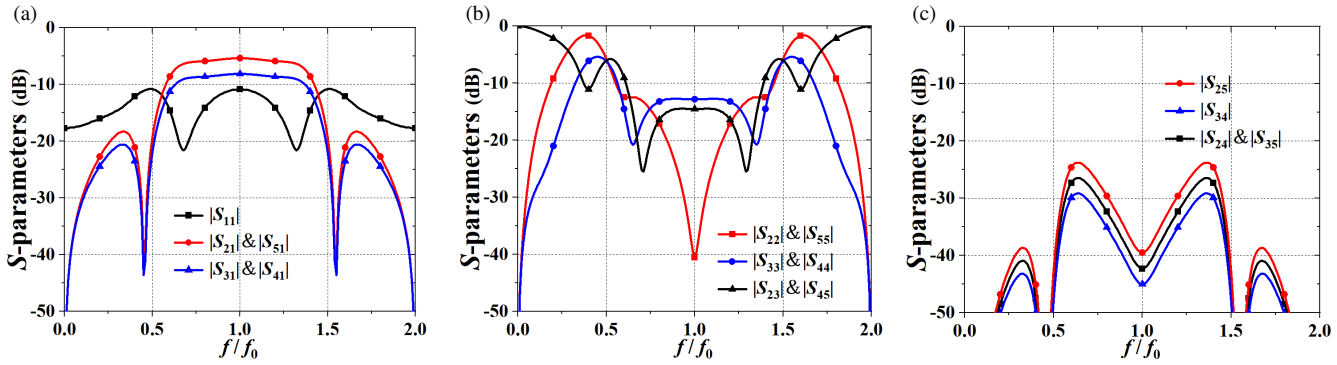

FIGURE 5. Theory results of the proposed four-way FPD. (a) $|S_{11}|$, $|S_{21}|$, $|S_{31}|$, $|S_{41}|$ and $|S_{51}|$. (b) $|S_{22}|$, $|S_{33}|$, $|S_{44}|$, $|S_{55}|$, $|S_{23}|$ and $|S_{45}|$. (c) $|S_{25}|$, $|S_{34}|$, $|S_{24}|$ and $|S_{35}|$.

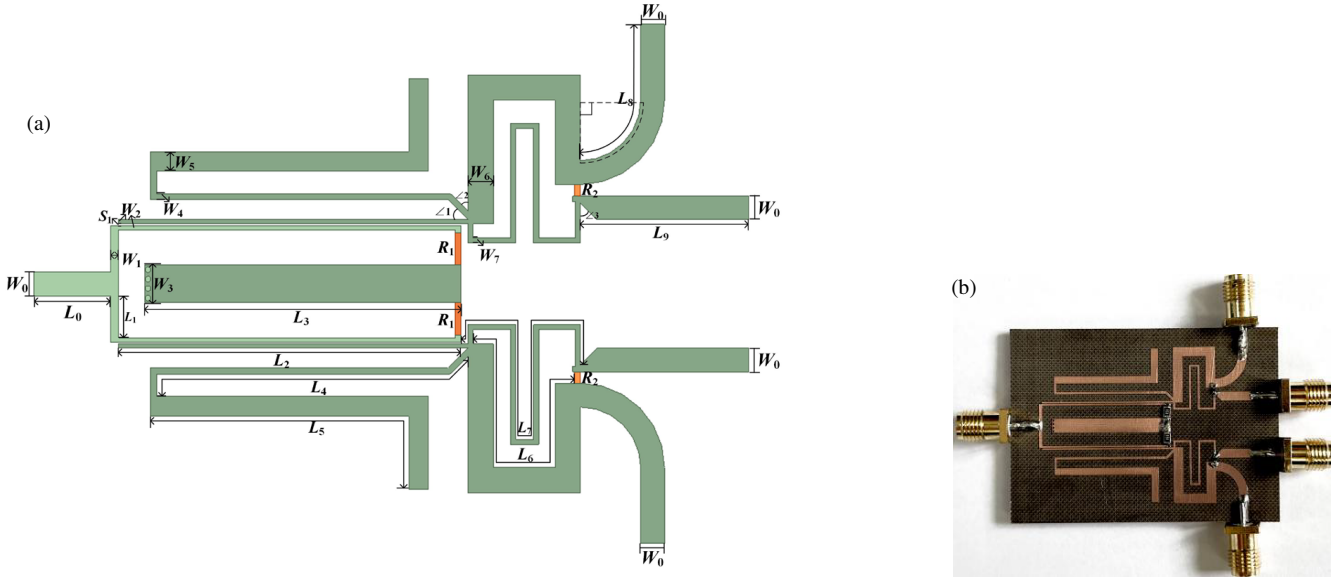

FIGURE 6. (a) Layout and (b) photograph of the fabricated FPD.

TABLE 1. The optimized dimensions of the prototype (Unit: mm).

W_0	W_1	W_2	W_3	W_4	W_5	W_6	W_7	S_1	R_1	R_2	L_0
1.7	0.56	0.3	2.7	0.44	1.4	1.8	0.36	0.12	140 Ω	120 Ω	5.44
L_1	L_2	L_3	L_4	L_5	L_6	L_7	L_8	L_9	$\angle 1$	$\angle 2$	$\angle 3$
3	24.4	22.5	24.8	25	22.8	23.4	12	11.7	45°	45°	45°

where the final dimensions are listed in Table 1. The overall size is 51 mm × 37 mm, yielding $0.62\lambda_g \times 0.46\lambda_g$.

Figure 7 shows the measured and simulated results. As seen from Fig. 7(a), the measured $|S_{11}|$ is greater than 10 dB from 0 to 4 GHz (200%). Due to the limited accuracy of welding instruments, there are some shifts of the good matching frequency for the measured results. However, it still maintains the absorptive bandwidth. Besides, the 3-dB FBW for ports 2 and 5 is 78.1% (1.14 ∼ 2.60 GHz) with a minimum IL of 0.65 dB at the center frequency. The 3-dB FBW for ports 3 and 4 is 79.4% (1.13 ∼ 2.62 GHz) with a minimum IL of 0.67 dB. The amplitudes for ports 2 and 5 ($|S_{21}|$ and $|S_{51}|$) are 5.42 dB, and the corresponding values for ports 3 and 4 ($|S_{31}|$ and $|S_{41}|$) are 8.45 dB, yielding a PDR of 2 : 1 : 1 : 2. Besides, the out-of-band rejections are larger than 14 dB at both upper and lower stopbands.

According to Fig. 7(b), the output ports 2 and 5 impedance matching characteristics are greater than 10 dB from 1.1 GHz to 2.68 GHz (83.6%). The output ports 3 and 4 impedance matching characteristics are greater than 10 dB from 1.1 GHz to 2.85 GHz (88.6%). Besides, the measured isolation between adjacent ports ($|S_{23}|$ and $|S_{45}|$) is greater than 15 dB from 1.4 GHz to 2.65 GHz (61.7%). Fig. 7(c) indicates that the measured isolations between non-adjacent ports are both greater

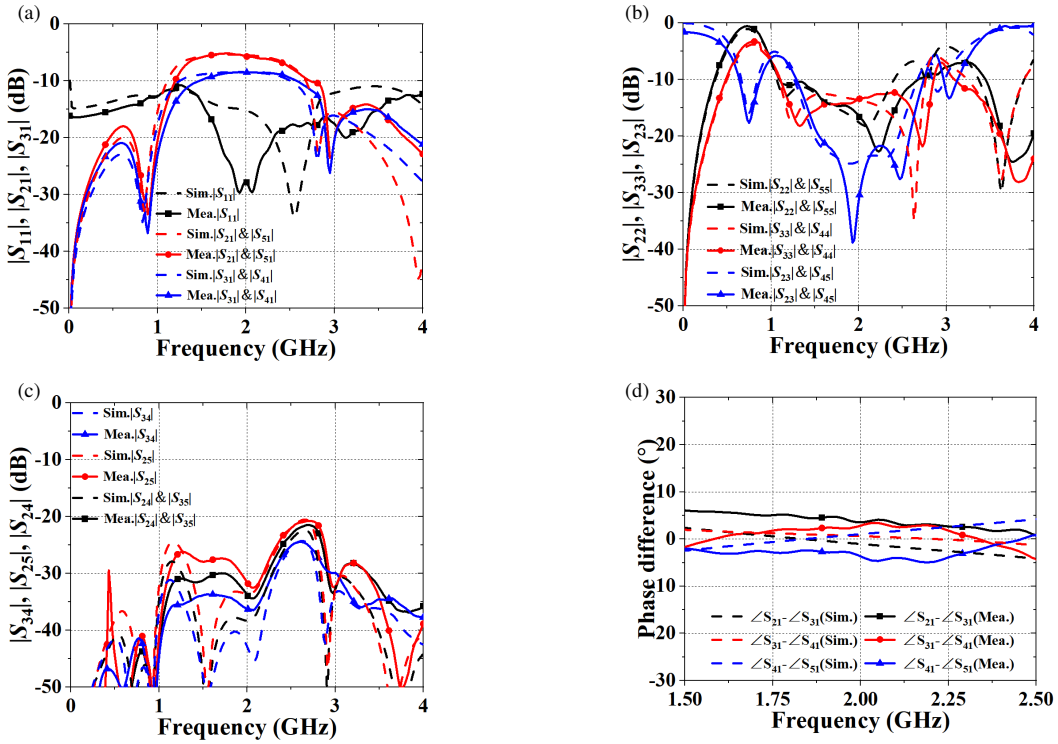

FIGURE 7. Simulated and measured results of fabricated prototype. (a) $|S_{11}|$, $|S_{21}|$, $|S_{31}|$, $|S_{41}|$ and $|S_{51}|$. (b) $|S_{22}|$, $|S_{33}|$, $|S_{44}|$, $|S_{55}|$, $|S_{23}|$ and $|S_{45}|$. (c) $|S_{24}|$, $|S_{25}|$, $|S_{34}|$ and $|S_{35}|$. (d) Phase difference (dash line: simulated results, line with symbol: measured results).

TABLE 2. Comparisons between the proposed rat-race coupler with related literatures.

Ref.		This work	[3]	[11]	[13]	[17]
Type		Unequal	equal	unequal	equal	equal
outputs		4	4	2	2	2
FBW(%)	$\lvert S_{11}\rvert < -10$ dB	200	106	250	250	250
	3-dB Passband	> 78.1	108*	> 82.5	52.8	55*
	10-dB ORFBW[a]	> 83.6	106	> 80	55	62.3
Isolation[b] (dB)		15	20	18	16	14.3
Stopbands (dB)		14	14	18	27	20
IL[c] (dB)		0.67	0.5	0.2	0.32	0.9
Absorption		Yes	No	Yes	Yes	Yes
Size ($\lambda_g \times \lambda_g$)		0.62×0.46	0.48×0.97	0.62×0.31	0.31×0.15	0.4×0.3

[a]. Output reflection FBW. [b]. Isolation of adjacent ports.
[c]. Minimum passband IL at the center frequency. *. Estimated from the results.

than 20 dB. It can also be seen from Fig. 7(d) that the measured phase differences between adjacent ports are $0° \pm 5°$.

Table 2 illustrates the performance comparisons between the proposed and representative related works. Although the FPD in [3] exhibits good performance, it can only realize equal power division, and does not have absorptive feature. Besides, the size of the circuit is large. The FPDs in [13] and [17] show small size, but they are two-way FPDs with equal power division. In [11], one unequal FPD with good absorptive feature is presented which shows similar dimension to the proposed structure. However, it has only two outputs, and the extension of four outputs will enlarge the size. Compared with [11], the proposed FPD can realize unequal power division under the premise of wideband filtering response, four-way outputs, input absorptive function, and small size.

4. CONCLUSION

The paper presents a wideband unequal four-way FPD with arbitrary power division ratio and input absorptive feature. Measurement and comparison results show that the proposed structure has the advantages of unequal power division, wideband, four-way output, input absorptive feature, and preferably frequency selectivity. It fills the gap of wideband unequal multi-

way absorptive FPD, which has potential applications in high-integrated modern wireless communication systems. In the future work, unequal FPDs (AFPDs) with small size, high frequency selectivity, and all-port absorptive feature will be focused on research.

ACKNOWLEDGEMENT

This work was supported in part by the National Natural Science Foundation of China under Grant 51809030, in part by the Liaoning Revitalization Talents Program under Grant XLYC2007067, in part by the Young Elite Scientists Sponsorship Program by CAST under Grant 2022QNRC001 and in part by the Fundamental Research Funds for the Central Universities under Grant 3132024239.

REFERENCES

[1] Hazeri, A. R., "An ultra wideband Wilkinson power divider," *International Journal of Electronics*, Vol. 99, No. 4, 575–584, 2012.

[2] Ding, Y., J. Wan, Y. Yan, and X. Liang, "A novel compact, wideband four-way Wilkinson power divider with an improved isolation topology," *IEEE Microwave and Wireless Technology Letters*, Vol. 33, No. 8, 1119–1122, Aug. 2023.

[3] Liu, Y., S. Sun, and L. Zhu, "2^n-Way wideband filtering power dividers with good isolation enhanced by a modified isolation network," *IEEE Transactions on Microwave Theory and Techniques*, Vol. 70, No. 6, 3177–3187, Jun. 2022.

[4] Zhu, C. and J. Zhang, "Design of high-selectivity asymmetric three-way equal wideband filtering power divider," *IEEE Access*, Vol. 7, 55 329–55 335, 2019.

[5] Song, K., L. Zhu, X. Xiong, and Y. Fan, "Wideband multi-channel multi-way power combiner with high frequency selectivity," *IEEE Transactions on Circuits and Systems II: Express Briefs*, Vol. 70, No. 4, 1376–1379, Apr. 2023.

[6] Liu, Y., S. Sun, and L. Zhu, "Design of n-way wideband filtering power dividers with good port-port isolation," *IEEE Transactions on Microwave Theory and Techniques*, Vol. 69, No. 7, 3298–3306, Jul. 2021.

[7] Zhang, G., Z. Liu, J. Yang, H. Wang, Q. Zhang, J. Shi, and W. Tang, "Wideband three-way filtering power divider on one single multimode patch resonator," *IEEE Transactions on Plasma Science*, Vol. 50, No. 9, 3270–3275, Sep. 2022.

[8] Guo, X., Y. Liu, and W. Wu, "Wideband unequal filtering power divider with arbitrary constant power ratio and phase difference," *IEEE Transactions on Circuits and Systems II: Express Briefs*, Vol. 70, No. 2, 421–425, Feb. 2023.

[9] Wang, D., X. Guo, and W. Wu, "Wideband unequal power divider with enhanced power dividing ratio, fully matching bandwidth, and filtering performance," *IEEE Transactions on Microwave Theory and Techniques*, Vol. 70, No. 6, 3200–3212, Jun. 2022.

[10] Chaudhary, G. and Y. Jeong, "Unequal power division ratio nonreciprocal filtering power divider with arbitrary termination impedance and center frequency tunability," *IEEE Transactions on Microwave Theory and Techniques*, Vol. 72, No. 1, 242–251, Jan. 2024.

[11] Zhang, S., H. Liu, S. Chen, Z. Wang, and S. Fang, "Wideband filtering power divider with unequal power division ratio and all-frequency input absorptive feature," *IEEE Transactions on Circuits and Systems II: Express Briefs*, Vol. 71, No. 3, 1136–1140, Mar. 2024.

[12] Li, Q., H. Tang, D. Tang, Z. Deng, and X. Luo, "Compact SIDGS filtering power divider with three-port 10-GHz reflectionless range," *IEEE Transactions on Circuits and Systems II: Express Briefs*, Vol. 69, No. 7, 3129–3133, Jul. 2022.

[13] Zhu, Y.-H., J. Cai, Y. Cao, and J.-X. Chen, "Compact wideband absorptive filtering power divider with a reused composite T-shape network," *IEEE Transactions on Circuits and Systems II: Express Briefs*, Vol. 70, No. 3, 899–903, Mar. 2023.

[14] Fan, M., K. Song, L. Yang, and R. Gómez-Garcia, "Frequency-reconfigurable input-reflectionless bandpass filter and filtering power divider with constant absolute bandwidth," *IEEE Transactions on Circuits and Systems II: Express Briefs*, Vol. 68, No. 7, 2424–2428, Jul. 2021.

[15] Gómez-García, R., J.-M. Muñoz-Ferreras, and D. Psychogiou, "RF reflectionless filtering power dividers," *IEEE Transactions on Circuits and Systems II: Express Briefs*, Vol. 66, No. 6, 933–937, Jun. 2019.

[16] Chaudhary, G., D. Lee, and Y. Jeong, "Group delay analysis approach for quasi-reflectionless power divider with flat phase difference," in *2021 IEEE Asia-Pacific Microwave Conference (APMC)*, 148–150, Brisbane, Australia, 2021.

[17] Zhang, Y., Y. Wu, J. Yan, and W. Wang, "Wideband high-selectivity filtering all-frequency absorptive power divider with deep out-of-band suppression," *IEEE Transactions on Plasma Science*, Vol. 49, No. 7, 2099–2106, Jul. 2021.

[18] Muraguchi, M., T. Yukitake, and Y. Naito, "Optimum design of 3-dB branch-line couplers using microstrip lines," *IEEE Transactions on Microwave Theory and Techniques*, Vol. 31, No. 8, 674–678, Aug. 1983.